www.czasopisma.pan.pl PAN POLSKA AKADEMIA NAUK www.journals.pan.pl

Arch. Metall. Mater. **65** (2020), 4, 1455-1462

DOI: 10.24425/amm.2020.133713

L. KUCHARIKOVÁ[1*], T. LIPTÁKOVÁ[1], E. TILLOVÁ[1], M. BONEK[2], D. MEDVECKÁ[1]

CORROSION BEHAVIOUR CORRELATION OF THE SECONDARY ALUMINIUM CASTS IN NATURAL ATMOSPHERE AND LABORATORY CONDITIONS

The secondary aluminium alloys are very important material in actual industry from economic and ecological point of view. The secondary aluminium used for production of casts, however, contains some elements, i.e. iron, – affecting physical, chemical and mechanical behaviour. The subject of our investigation has been corrosion behaviour in natural atmosphere of the hypoeutectic AlSi7Mg0.3 cast alloys with various content of iron, because the Fe content affects not only mechanical properties but corrosion resistance, as well. Three types of the AlSi7Mg0.3 cast alloys were exposed for 9 months in natural atmosphere and the measure of their degradation by corrosion was found by determination of the weight loss and the light microscopy. In addition, a scanning electron microscopy (SEM) analyses and evaluation of surface changes were used. The corrosion behaviour in natural atmosphere was compared to results of the carried out electrochemical and exposure laboratory experiments in chloride solutions.

Keywords: secondary aluminium alloys, high Fe content, corrosion properties, natural atmosphere

1. Introduction

A large increase of aluminium alloys in transport casts and constructions has taken place in the last decades. The advantages of their utilization are especially improving the fuel economy, energy consumption and decrease of the harmful gases emission [1-6]. Because of various industrial applications and economic importance of aluminium alloys, their mechanical properties were studied in many research works; however the corrosion ones did not receive so much attention [7-9]. The majority of aluminium alloys have naturally good corrosion resistance in real atmospheres and many other environments, because aluminium alloy surfaces are covered with a natural protective Al oxide film of thickness of about 5 nm [10]. This film is resistant to attack from water and oxygen in a wide range of temperatures [11]. However, the typical forms of corrosion, occurring in aluminium alloys (in an aquatic environment enriched with halogens, mainly chlorides, with pH values between 4 and 8), are localized forms of corrosion (pitting corrosion, intergranular corrosion and layered corrosion). Out of these three types, the pitting corrosion is the main one [12].

Many research studies [6,13-15] demonstrated that localized corrosion susceptibility of aluminium alloys is related to presence of the second-phase particles (intermetallic phases) in the alloy, the potential formation of which is depending on the casting conditions, solidification rate, as well as on chemical composition. In addition, it is noticed that the electrochemical behaviour of the second-phase particles depends mainly upon difference between the particle and the matrix. The important phases are: α-matrix (dendrite cell size, dendrite arm spacing-SDAS, and grain size), eutectic silicon particles and intermetallic phases (size, morphology, and amount) and also porosity [7-9,13]. The presence of higher amount of Si (which induces a major precipitation of Mg_2Si) causes the higher intergranular corrosion susceptibility. During the corrosion, Mg_2Si has an anodic behaviour with respect to the Al-rich phase, promoting anodic dissolution and surface corrosion [6,11,12,14-17]. The Si and Fe-containing phases (β-AlFeSi or α-AlFeSiMg) are cathodic with respect to the Al matrix forming micro-galvanic couples [14,16]. All the presented scientific works confirmed that the electrochemical behaviour of the alloys is closely related to their microstructure.

From the Fe-rich phases, identified in the Al-Si base alloys, the α-$Al_{15}FeMn_3Si_2$ and β-Al_5FeSi phases are being the more important [18-20]. The β-phases crystallize as thin plates that in the cross section look like needles. The iron content determines the shape of these needles, which are brittle and have relatively little coherence with the aluminium matrix. From the electrochemical point of view, the β-Al_5FeSi phase is nobler than the matrix in

[1] UNIVERSITY OF ŽILINA, FACULTY OF MECHANICAL ENGINEERING, UNIVERZITNÁ 8215/1, 010 26 ŽILINA, SLOVAKIA
[2] SILESIAN UNIVERSITY OF TECHNOLOGY, INSTITUTE OF ENGINEERING MATERIALS AND BIOMATERIALS, KONARSKIEGO 18A, 44 100 GLIWICE, POLAND

* Corresponding author: lenka.kucharikova@fstroj.uniza.sk

aqueous media, making the alloy system highly susceptible to localized corrosion. The different Fe-rich intermetallic phases have similar corrosion potentials and thus a comparable pitting formation [20,21].

Since the corrosion properties have a vital effect on the properties and lifetime of construction components, the aim of this work is a study of the corrosion behaviour of the secondary aluminium alloy AlSi7Mg0.3 with different amounts of Fe in natural atmosphere and compare to their corrosion behaviour in the chloride environments, tested in laboratory conditions.

2. Experimental procedure

The experimental alloy was the hypoeutectic AlSi7Mg0.3 cast alloy. However, the increased usage of recycling possibilities, caused that this material was produced with different the iron concentration (0.123 % Fe – alloy A, 0.454 % Fe – alloy B, 0.655 % Fe – alloy C). The chemical composition of the experimental alloys was quantified using spectroscopy analysis on SPECTROMAXx and is shown in Table 1.

These types of experimental materials have excellent castability, good corrosion and wear resistance, high strength stiffness to weight ratio (good mechanical properties), low density and thermal expansion, high productivity and low shrinkage rate, recycling possibilities and low costs. Therefore, they can be given a wide variety of surface finishes and can be cast and produced into almost any form of product [5,6].

Mechanical properties were measured according to the following standards: ISO 6892-1:2009, and STN EN ISO 6506-1. Hardness measurement for experimental alloy was performed on the polished samples by using the Brinell hardness tester with load of 250 kp (1 kp = 9.80665 N), testing ball of 5 mm diameter and a dwell time of 15 s (mark is: HBW 5/250/15). The ultimate tensile strength was measured using the INSTRON Model 5985 testing machine. The dimensions of testing specimens were: the cross section ø 10 mm and initial measured length 50 mm. The resulting Brinell hardness value and ultimate tensile strength value are arithmetic mean of six separate measurements. All the tests were performed at ambient temperature (~22°C).

The optical microscope Neophot 32 and SEM were used for assessment of morphology changes of structural parameters and the corrosion attack. Samples for optical microscopy were prepared by standard metallographic procedures (wet ground by SiC papers, DP polished with 3 μm diamond pastes followed by Struers Op-S and etched for study at an optical microscope by etchant reagents 0.5% HF for common evaluation and H_2SO_4 for highlighting of the Fe-rich intermetallic phases).

3. Results and Discussion

3.1. Microstructure

According to the binary Al-Si phase diagram, the experimental material belongs to hypoeutectic aluminium cast alloys and the microstructure is created by dendrites of a matrix and eutectic [22] (Fig. 1). The matrix is the solid solution of Si in Al (α-Al, α-phase) and the eutectic (E) is mechanical mixture of matrix and eutectic Si (Fig. 1a). Small amounts of impurity like

TABLE 1

The chemical composition measured by the arc spark spectroscopy, wt. [%]

Alloy	Si	Fe	Cu	Mn	Mg	Zn	Ti	Na	Al	Other
A	7.028	**0.123**	0.013	0.009	0.354	0.036	0.123	0.002	92.253	balance
B	7.34	**0.454**	0.021	0.009	0.302	0.02	0.118	0.004	91.673	balance
C	7.315	**0.655**	0.03	0.01	0.292	0.028	0.12	0.005	91.486	balance

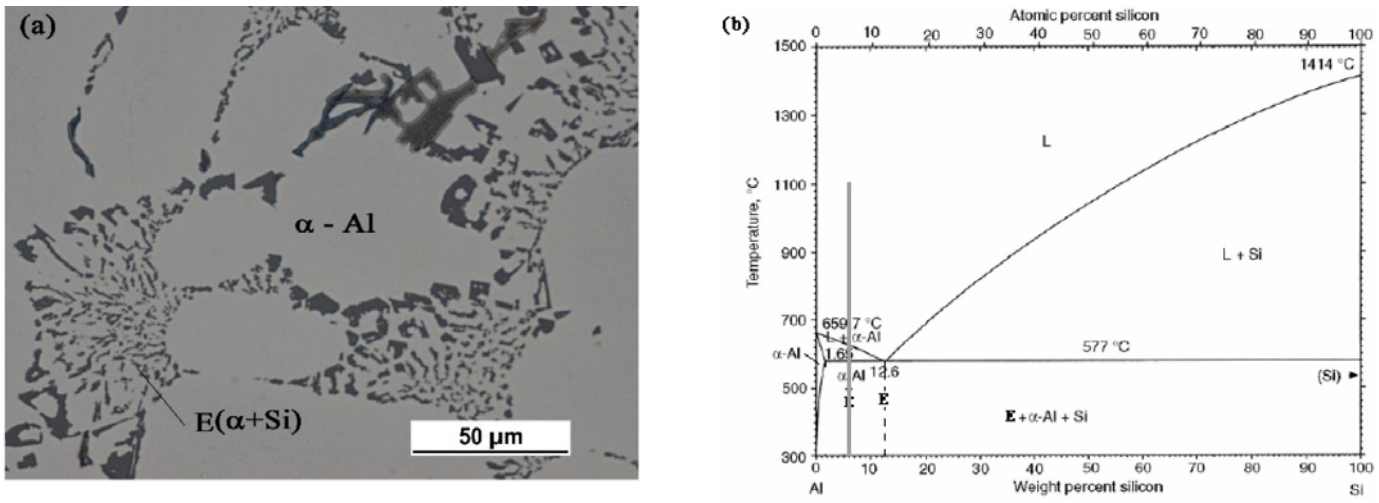

Fig. 1. The basic microstructure (a) according to phase binary diagram of A-Si [22] (b)

iron are quite common in commercial alloys. These impurities are products of the refining and smelting processes [22]. Therefore, aluminium cast alloys besides basic microstructural features (eutectic and matrix) contain intermetallic phases determined by chemical composition of alloys. The maximum solubility of Fe in Al alloys is 0.05 wt. %; however, in commercial alloys the solubility is lower. The low amount of Fe leads to forming the Al_3Fe intermetallic phases with a monoclinic crystal structure. If manganese is also present and depending on the solidification rate, the Al_6Fe may precipitate instead of previous phases.

However, commonly used Al-Si cast alloys (with higher amount of Si) may have two types of Fe-rich intermetallic phases by a eutectic reaction: α-$Al_xFeMn_xSi_x$ (cubic crystal structure) and β-Al_xFe_xSi (monoclinic crystal structure) [23-25].

Observation and assessment of basic microstructure of experimental AlSi7Mg0.3 cast alloy showed that each experimental materials contains Fe-rich intermetallic phases in needles form: Al_5FeSi, and in form of skeleton-like or Chinese script: $Al_{15}(FeMg)_2Si_2$ and Mg-rich intermetallic phases: Mg_2Si (Fig. 2) in form of skeleton-like. The increasing amount of Fe in experimental alloys (B and C) leads to formation of larger amount of the Fe-needles intermetallic phases (Fig. 3) and the length and thickness were different, as well. The alloy A has the average length of the Fe-rich needles 24.49 µm the alloy B have of about 30% (35.43 µm) larger length of these phases and alloy C of about 42% (41.93 µm). The volume fraction of the needles also increases with higher amount of Fe in the experimental alloys: alloy A 1%, alloy B 2.3% and alloy C 2.6%. The formation of the Mg rich phases was affected too. The Mg rich phases were smaller and their amount was also decreasing. The formation of the Fe-rich phases $Al_{15}(FeMg)_2Si_2$ was similar as in the Mg-rich phases.

The porosity assessment also confirms the effect of the Fe-rich needles on increasing the pore size and volume fraction, as it was reported in the Sacinty research work [23] (Fig. 4). The maximum area size of porosity was measured for materials with the highest amount of Fe – the alloys C (219 627 µm^2) and the maximum volume fraction of porosity for the alloys B (5.6%). The alloys with the amount of Fe corresponding to standards have the volume fraction 3.8% and area size 125 723 µm^2.

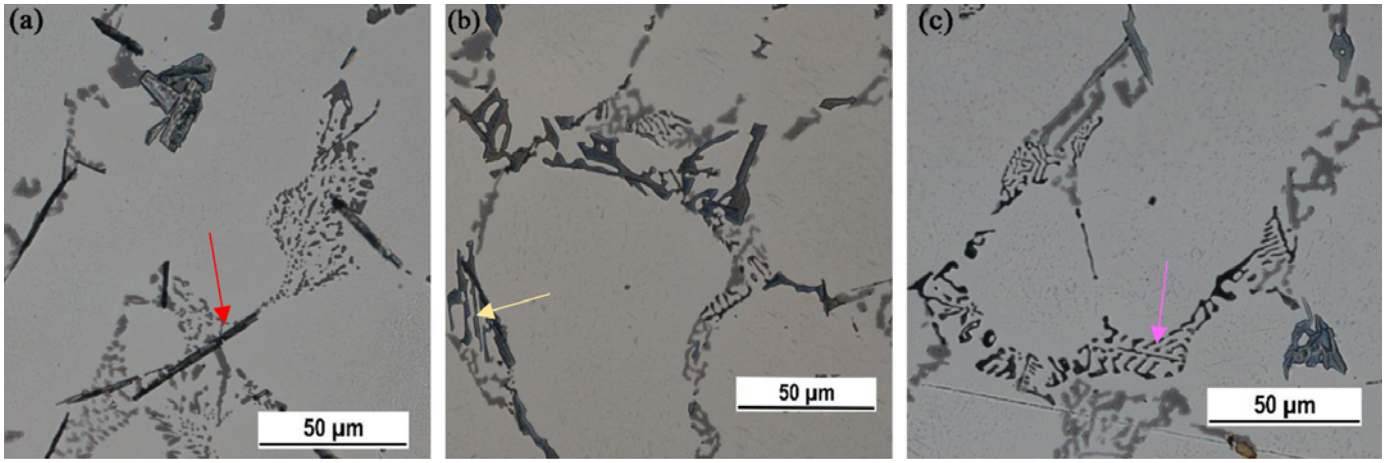

Fig. 2. Intermetallic phases in experimental cast alloys. (a) Fe-rich intermetallic phases Al_5FeSi; (b) Fe-rich intermetallic phases $Al_{15}(FeMg)_2Si_2$; (c) Mg-rich intermetallic phases Mg_2Si

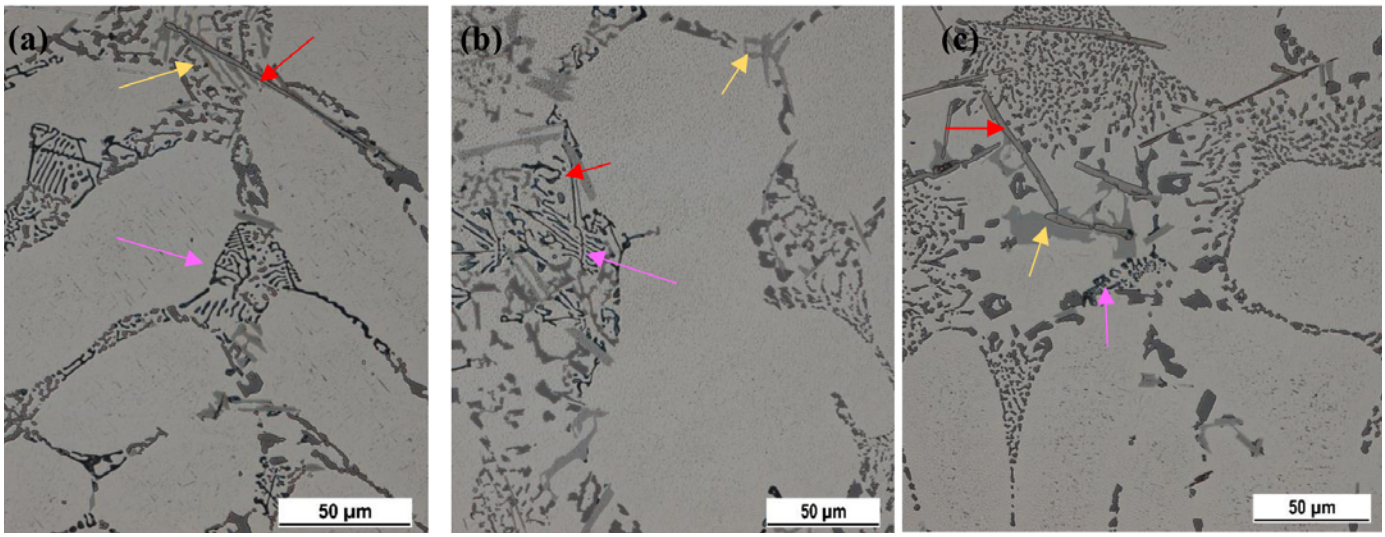

Fig. 3. Effect of the higher amount of Fe on microstructure of experimental alloys. (a) alloy A; (b) alloy B; (c) alloys C

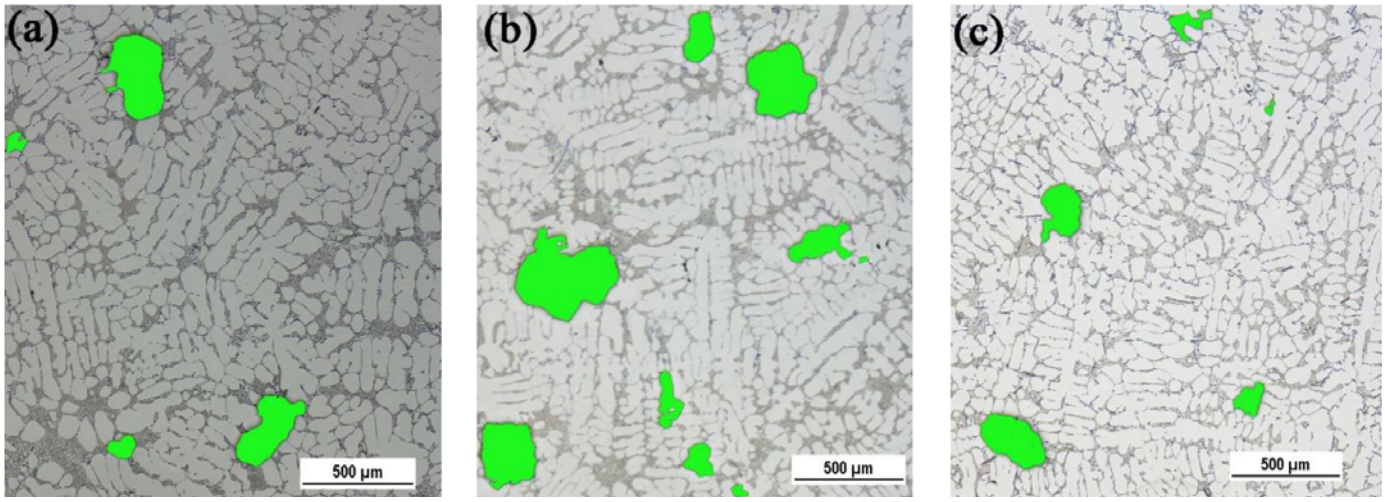

Fig. 4. Effect of the higher amount of Fe on porosity formation. (a) alloy A (b) alloy B (c) alloys C

3.2. Mechanical properties

Increasing of the Fe amount did not affect negatively measured mechanical properties of the tested alloys (Table 2). The differences were of about 5 to 7%, which is the value of common measurements' errors for mechanical properties of casted materials.

TABLE 2

Results of mechanical properties of experimental materials

Alloy	A	B	C
UTS [MPa]	140	150	147
HBW 5/250/15	52	55	54
Ductility [%]	1.45	1.91	1.58

3.3. Corrosion behaviour

The corrosion behaviour of the secondary hypoeutectic AlSi7Mg0.3 cast alloys with different iron concentration was investigated. The samples were exposed for nine months in the natural atmosphere according to the standard ISO 8565: 2011. The atmosphere was defined according to the standards STN EN ISO 9223: 2012 and STN EN ISO 9224: 2012. The average parameters during the exposure were: temperature = 9.5°C, relative humidity (%) = 75, SO_2 content ($\mu g.m^{-3}$) = 12, NO_x content ($\mu g.m^{-3}$) = 25, pH of precipitation – 6 [26]. The samples shape was a cylinder with turned surface and with the porosity parameters mentioned before. The morphology of the samples surface was visually investigated before testing because their character and real area size affect corrosion rate. In spite of the fact that the samples were turned before testing under the same conditions, some morphology disparities were observed (Fig. 5). That was confirmed by surface roughness parameters Ra and Rz (Ra – the average roughness of a surface and Rz – the difference between the tallest "peak" and the deepest "valley" in the surface) before and after exposure, as well as the weight losses (Table 3).

TABLE 3

Weight losses and roughness of the AlSi7Mg0.3 alloys with different content of Fe in the longitudinal direction

Alloy	A		B		C	
Exposure	before	after	before	after	before	after
Ra (µm)	0.925	0.8826	1.52	1.142	1.481	1.108
Rz (µm)	6.1287	5.6785	8.927	7.458	9.662	7.117
Weight. Loss (g)	–0.0005		–0.00087		–0.00063	

Roughness of the samples decreases after exposure in atmosphere what can be caused by fulfilling the surface undulation by corrosion products and atmosphere impurities. According to results, it can be said that the corrosion intensity is slightly affected by the higher Fe content (0,454 and 0,655%).

The weight losses differ very slightly and do not provide relevant information on the corrosion rate because character of corrosion is mostly local (Fig. 6, 7) and is affected by the chemical composition of corrosion products, as well as by surface roughness (Table 3) of the tested alloys. In Fig. 6 it can be seen the more intensive corrosion attack in places with the present Si rich phases, of the cathodic character. It was confirmed by the EDX analysis of the surface, where oxygen and sulphur concentration in corrosion product is accumulated between the Si rich phases of the cathodic character.

In alloys with the higher content of iron the needles (with high Fe concentration) penetrate the surface. In spite of the fact they are considered cathodic to the matrix (not to the surface), the corrosion products of Fe were identified by the EDX analysis (Fig. 7). The presence of the Fe corrosion products was visually observed like brown spots on the grey surface. It can also influence weight losses. The corrosion attack of the sample was very similar from both the qualitative and quantitative points of view. The exposure in natural atmosphere was not long, but starting corrosion rate is determining for the corrosion rate after corrosion process stabilization [24].

On the contrary, the negative effect of the Fe content in the AlSi7Mg0.3 alloys was demonstrated by the exposure testing

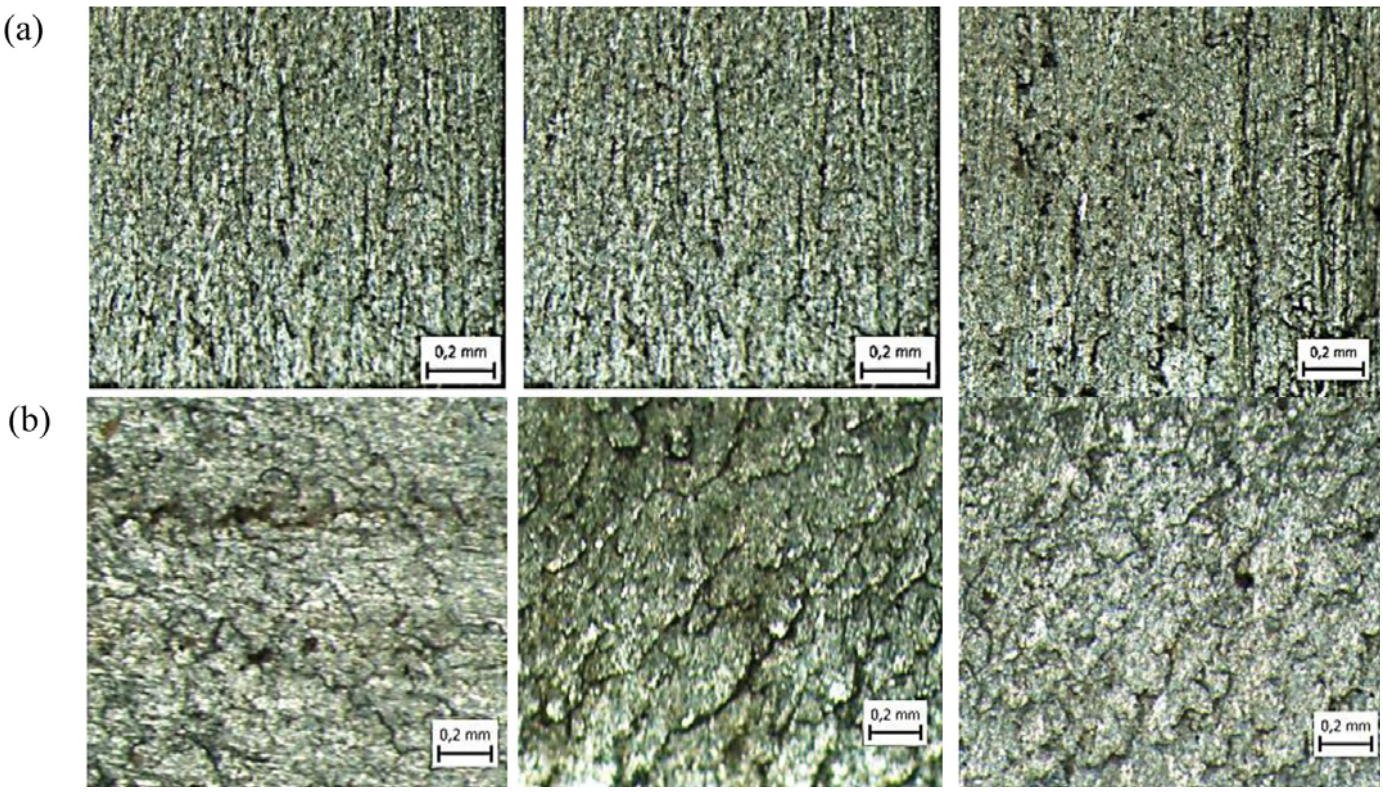

Fig. 5. The surface morphology of the experimental secondary alloys with different Fe content before (a) and after (b) exposure

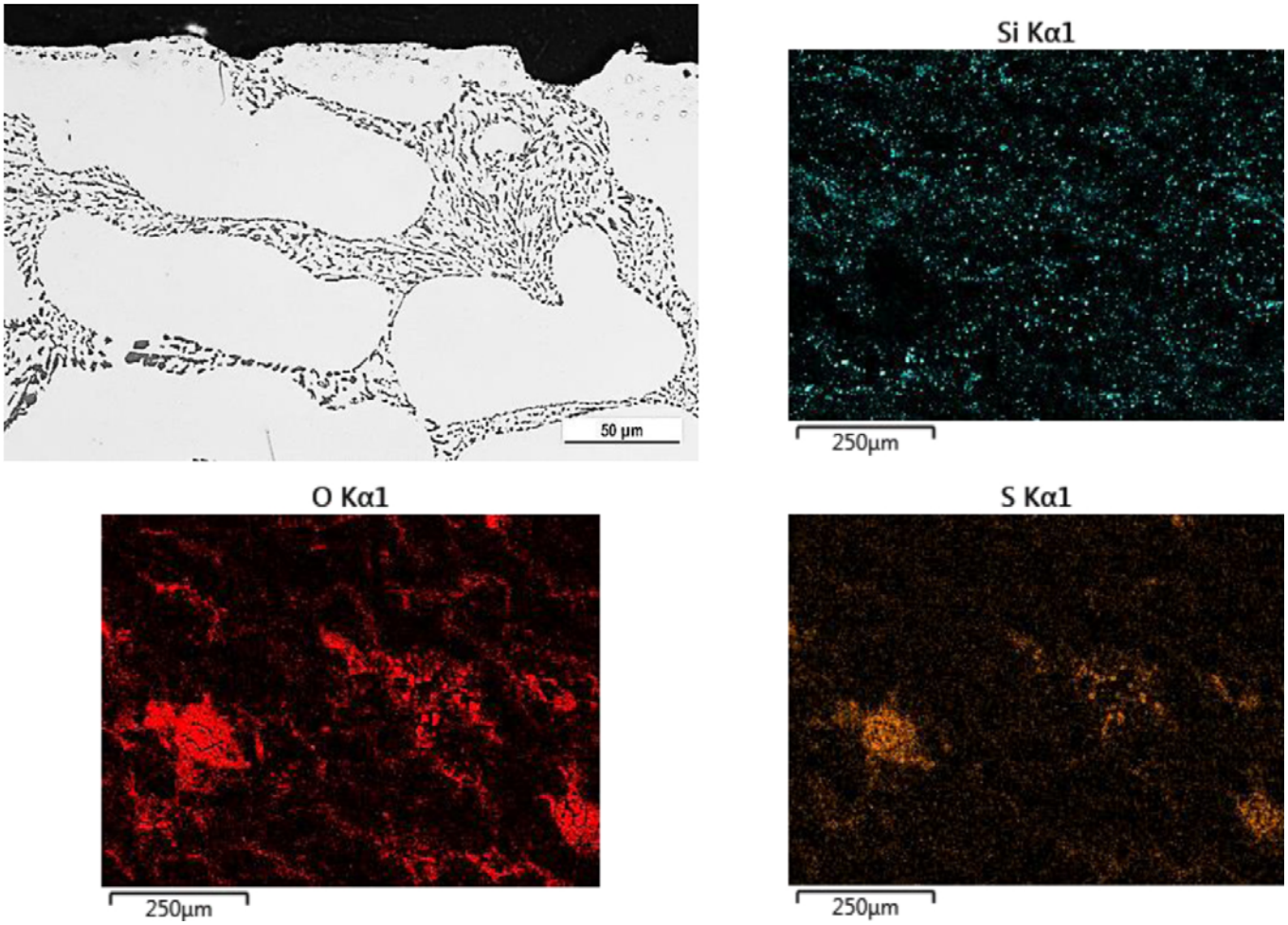

Fig. 6. Corrosion of the sample A in localities of eutectic Si phases or eutectic supported by the EDX analysis

in the 3.5 wt.% NaCl solution at 20°C for three weeks, according to conditions in [27]. The differences of the local corrosion intensity can be observed in Fig. 8. Susceptibility to local corrosion in chloride environment grows with the Fe content markedly.

In addition, potentiodynamic test, carried out in the 3.5% sodium chloride solution [27] reflects the Fe concentration in the AlSi7Mg0.3 alloy. The corrosion potential E_{corr} of all the AlSi7Mg0.3 alloys with different contents of iron, drops with increasing its content (Fig. 9). At the concentration of the Fe 0,454 and 0.655 wt. % the experimental alloys show the lower corrosion stability in comparison to the alloy containing 0.123% Fe.

4. Conclusion

The study of the Fe content effect on the corrosion behaviour of the AlSi7Mg0.3 cast alloys shows:

- The assessment of microstructure confirms formation of higher amount of Fe needles phases in experimental materials with increasing content of Fe.
- The mechanical properties of experimental materials with higher content of Fe (alloy B and C) were similar to material with content Fe according to standards (alloy A).
- Influence of the Fe content on corrosion behaviour of the AlSi7Mg0.3 – alloys in natural atmosphere is not very marked in comparison to weight loss and intensity of local corrosion. The increasing Fe concentration was demon-

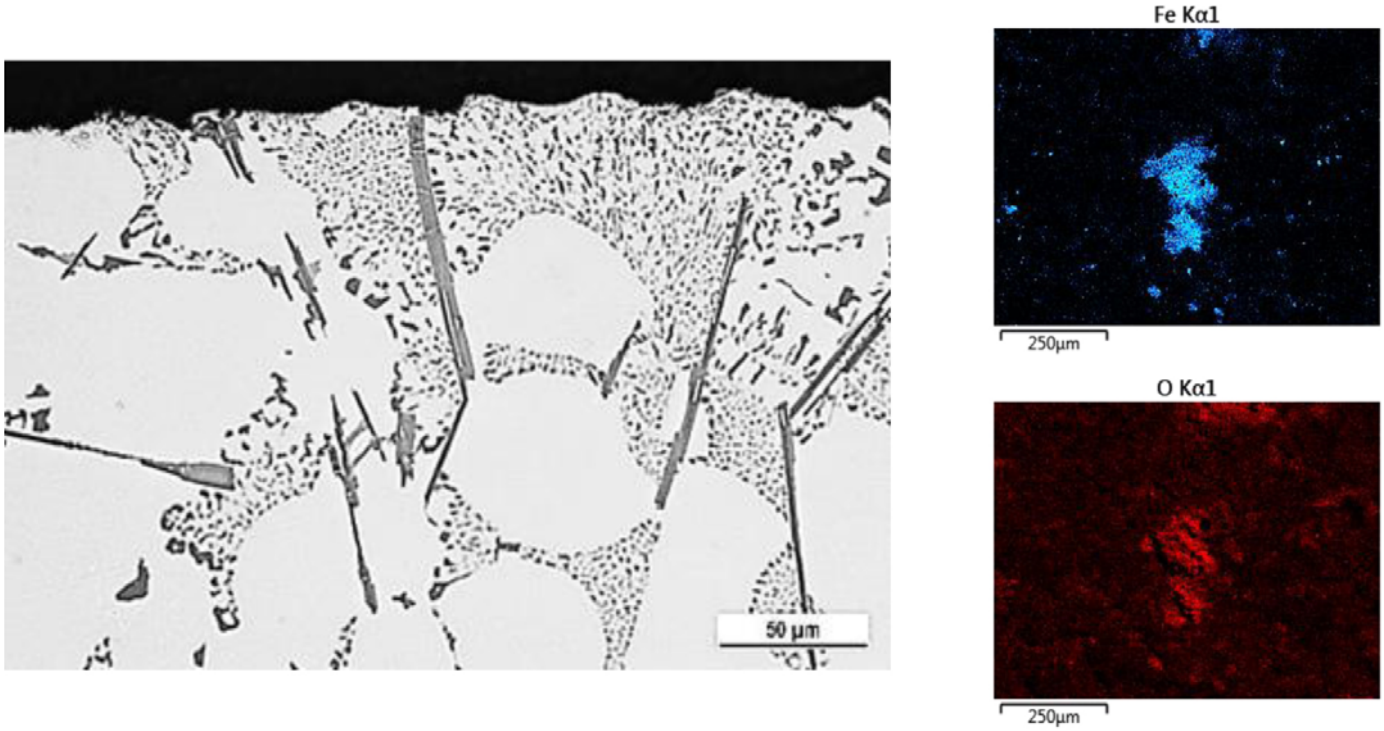

Fig. 7. Localization of needls on the surface and the EDX analysis of the corrosion product of sample C in this locality

Fig. 8. The corrosion character of the tested alloys after exposure test

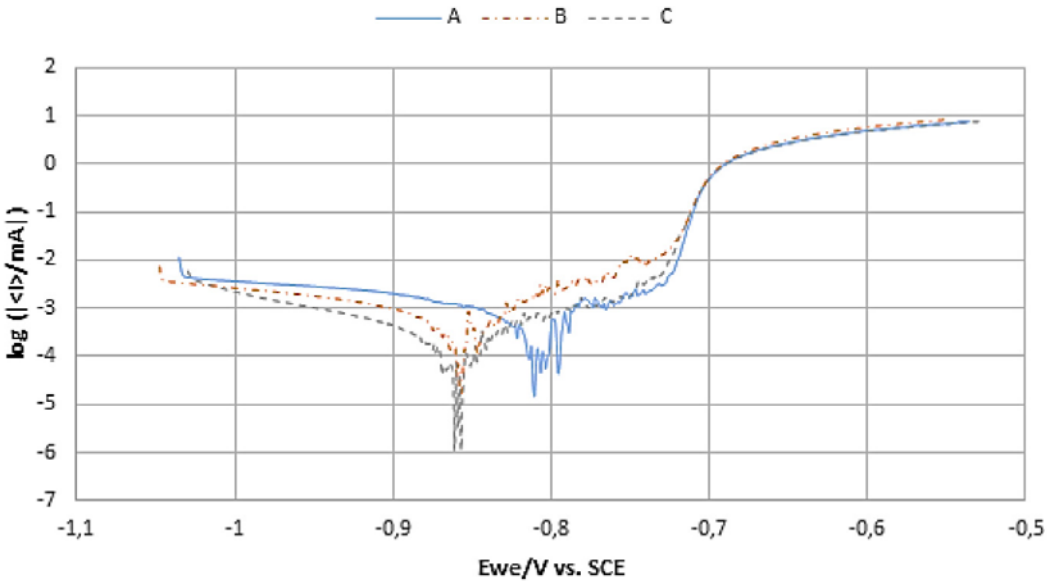

Fig. 9 Potentiodynamic curve of the tested Al-alloys with various Fe content

strated in the brown spots density in the sample surfaces of the Fe corrosion products. Their size was less than a mm.

- On the contrary, in the chloride solutions the increasing Fe content evidently affected the susceptibility to local corrosion and also its intensity.

Acknowledgement

This work was supported under the projects: of the Scientific Grant Agency of the Ministry of Education, Science and Sports of the Slovak Republic Academy of Science No 1/0398/19 and No 049ŽU-4/2017, in addition by project of Operational Program Research and Innovation: "Research and development activities of the University of Žilina in the Industry of 21st century in the field of materials and nanotechnologies", No. 313011T426. The project is co-funded by European Regional Development Fund. The publication is the result of bilateral cooperation within the Polish National Agency of Academic Exchange. The publication was co-financed from the statutory grant of the Faculty of Mechanical Engineering at the Silesian University of Technology in 2019.

REFERENCES

[1] A. Bialobrzeski, J. Pezda, A. Jarco, Arch. Metall. Mater. **62**/4, 2371-2374 (2017). DOI: 10.1515/amm-2017-0349

[2] J. Hirsch, T. Al-Samman, Acta Materialia **61**, 818-843 (2013), https://doi.org/10.1016/j.actamat.2012.10.044

[3] C. Cai, H. Geng, S. Wang, B. Gong, Z. Zhang, Materials (Basel). **11**/5, 809-822 (2018). DOI:10.3390/ma11050809

[4] T. Tański, K. Labisz, B. Krupińska, M. Krupiński, M. Król, R. Maniara, W. Borek, Journal Therm Anal Calorim. **123**/1, 63-74 (2016). DOI 10.1007/s10973-015-4871-y

[5] N. Náprstková, J. Cais, Production Engineering Archives **3**/2, 10-13 (2014).

[6] R.A. Rodríguez-Diaz, J. Uruchurtu-chavarín, A.M. Cotero-Villegas, S. Valdez, J.A. Juárez-Islas, Int. J. Electrochem. Sci. **10**, 1792-1808 (2015)

[7] W.R. Osório, P.R. Goulart, A. Garcia, Materials Letters **62**, 365-369 (2008).

[8] W.R. Osório, N. Cheung, J.E. Spinelli P.R. Goulart, A. Garcia, Journal Solid State Electrochem. **11**, 1421-1427 (2007).

[9] S. Cecchel, G. Cornacchia, M. Gelfi, Materials and Corrosion **68**, 961-969 (2017).

[10] M. Kliskic, J. Radosevic, S. Gudic, V. Katalinic, Journal of Applied Electrochemistry **30**, 823-830 (2000).

[11] R. Escalera-Lozano, M.I. Pech-Canul, M.A. Pech-Canul, M. Montoya-Dávila, A. Uribe-Salas, The Open Corrosion Journal **3**, 73-79 (2010).

[12] F. Ostermann, Springer-Viewer Verlag. **S. 233**. (2015) ISBN: 978-3-662-43806-0

[13] E. Linardia, R. Haddad, L. Lanzan, Procedia Materials Science **1**, 550-557 (2012).

[14] S. Jain, The Ohio State University; Columbus, OH, USA: 2006. PhD. Thesis with title: Corrosion and Protection of Heterogeneous Cast Al-Si (356) and Al-Si-Cu-Fe (380) Alloys by Chromate and Cerium Inhibitors.

[15] K.A. Yasakau, M.L. Zheludkevich, S.V. Lamaka, M.G.S. Ferreira, Electrochim. Acta **52**, 7651-7659 (2007). DOI: 10.1016/j.electacta.2006.12.072

[16] P. Chen, L.H. Liang et al., Advanced Materials Research **900**, 96-99 (2014). DOI: 10.4028/www.scientific.net/AMR.900.96.

[17] F.L. Zeng, Z.L. Wei et al., Transactions of Nonferrous Metals Society of China. **21**/12, 2559-2567. (2011). DOI: 10.1016/S1003-6326(11)61092-3

[18] A.M. Samuel, F.H. Samuel, H.W. Doty, S. Valtierra, International Journal of Metalcasting **12**/1, 55-70 (2018).

[19] W. Khalifa, F.H. Samuel, J.E. Gruzleski, Metall. Mater. Trans. **A 34**, 807-825 (2003).

[20] J.A. Taylor, G.B. Schaffer, D.H. Stjohn, Metallurgical and Materials Transactions **30A**, 1651-1655 (1999).

[21] S. Cecciel, G. Cornacchia, M. Gelfi, Materials and Corrosion **68**, 931-969 (2017). DOI: 10.1002/maco.201709526

[22] L. Kuchariková, E. Tillová, M. Matvija, J. Belan, M. Chalupová, Arch. Metall. Mater. **62**/1, 397-103 (2017). DOI: 10.1515/amm-2017-0062

[23] M. Sacinti, E. Cubuklusu, Y. Birol, International Journal of Cast Metals Research **30**/2, 96-102 (2017).

[24] L. Hurtalová, E. Tillová, M. Chalupová, Metalurgija **54**/1, 39-42 (2015).

[25] L. Hurtalová, E. Tillová, M. Chalupová, Materials Science Forum **782**, 359-364 (2014).

[26] K. Kreislová, D. Knotková, Materials **10**, 394-404 (2017).

[27] S. Sun, Q. Zheng, D. Li, J. Wen, Corrosion Science **51**, 719-727 (2009).

[28] L. Kuchariková, T. Liptáková, E. Tillová, D. Kajánek, E. Schmidová, Metals **8**/8, 581 (2018).